Time-dependent subsidence associated with drainage-induced compaction in Gulf of Mexico shales bounding a severely depleted gas reservoir

Chandong Chang, Ellen Mallman, and Mark Zoback

ABSTRACT

Production from ubiquitous oil and gas fields in coastal Louisiana and consequent reservoir compaction has been proposed as an important process contributing to coastal subsidence and land loss in this region. As revealed by three consecutive leveling surveys (in 1965, 1982, and 1993), an unexpected aspect of the subsidence is that the rate of subsidence actually increased after the cessation of production. To explain the accelerated postdepletion subsidence, we propose a mechanism involving time-dependent drainage and compaction in the overlying and underlying shales after depletion. We show that the shale compaction is induced by slow drainage of pore fluid from the shale to the depleted reservoir. We estimate the significance of postdepletion compaction in the bounding shale using a relatively simple analytic model in which time-dependent shale compaction is driven by pore pressure diffusion with two sets of rheological constitutive equations: one accounting for poroelastic effects and one accounting for viscoplastic deformation of the shale matrix. Our modeling shows that despite its very low permeability, after about 10 years, vertical compaction due to pressure drainage in the shale exceeds that due to depletion and compaction of the sand reservoir. Consequently, the calculated subsidence rate due to the shale compaction is higher than the subsidence induced by reservoir depletion, thus demonstrating that postdepletion compaction in the reservoir-surrounding shale may explain the observed acceleration of subsidence after depletion.

Manuscript received January 10, 2013; provisional acceptance June 10, 2013; revised manuscript received July 10, 2013; final acceptance November 11, 2013.
DOI: 10.1306/11111313009

AUTHORS

CHANDONG CHANG ~ *Department of Geology, Chungnam National University, Daejeon 305-764, South Korea; cchang@cnu.ac.kr*

Chandong Chang is a professor of engineering geology at Chungnam National University, South Korea. Dr. Chang received B.S. and M.S. degrees in geophysics from Seoul National University, and a Ph.D. in geological engineering from the University of Wisconsin-Madison. He has research interests in a wide range of geomechanics including in situ stress, rheology, and fault and earthquake mechanics.

ELLEN MALLMAN ~ *Department of Geophysics, Stanford University, Stanford, California 94305; present address: BP, 1-4 Wellheads Avenue, Dyce, Aberdeen AB21 7PB, UK; Ellen.Mallman@uk.bp.com*

Ellen Mallman received her Ph.D. in geophysics from Stanford University in 2007 where she focuses on the role of hydrocarbon production in subsidence and land loss in southern Louisiana. She currently is working for BP as a geomechanics and pore pressure specialist for the North Sea in Aberdeen, Scotland.

MARK ZOBACK ~ *Department of Geophysics, Stanford University, Stanford, California 94305; zoback@stanford.edu.*

Mark D. Zoback is the Benjamin M. Page Professor of Geophysics at Stanford University. Zoback conducts research on in situ stress, fault mechanics, and reservoir geomechanics with an emphasis on shale gas, tight gas, and tight oil production. He is the author of a textbook entitled *Reservoir Geomechanics*, first published in 2007 by Cambridge University Press.

ACKNOWLEDGEMENTS

Chandong Chang thanks the Blaustein Visiting Professor fund from the Stanford School of Earth Sciences and the Stanford Rock Physics and Borehole Mechanics Consortium for being able to conduct this research. We appreciate the thoughtful reviews provided by David Awwiller, Paul

Hagin, and Torbjörn Törnqvist, who helped enhance the quality of this manuscript.

The AAPG Editor thanks the following reviewers for their work on this paper: David N. Awwiller, Paul Hagin, and Torbjörn Törnqvist.

INTRODUCTION

Coastal Louisiana is experiencing high rates of regional-scale land subsidence (Shinkle and Dokka, 2004; Morton et al., 2006). The subsidence rates vary spatially and temporally with magnitudes as high as a few tens of millimeters per year in some areas. These exceptionally high rates of subsidence are believed to cause serious societal problems in the region, such as continuing wetland loss (Penland et al., 2000; Morton et al., 2003) and shoreline changes (Fearnley et al., 2009). Understanding the mechanism of subsidence benefits its prediction and management.

Previous studies have investigated several possible mechanisms that can induce such widespread and significant subsidence prevailing in this region (Dokka, 2006; Meckel et al., 2006; Morton et al., 2006). Some representative natural processes are compaction of Holocene sediments deposited in the Mississippi River delta plain (Meckel et al., 2006; Törnqvist et al., 2008), lithospheric flexure in response to the sediment load (Scardina et al., 1981), and faulting in the tectonically extensional environment (Dokka, 2006). However, subsidence rates due to these natural processes are estimated to be significantly lower (<5 mm/yr [0.2 inch/yr]) than the observed historical rates of 9 mm/yr (0.35 inch/yr) to as high as 23 mm/yr (0.9 inch/yr) locally (Morton et al., 2002). Although previous studies tended to focus only on a specific mechanism, it seems clear that subsidence in the region likely results from a combination of multiple mechanisms associated with natural and anthropogenic processes.

More fine-scale comparisons between spatial variation of subsidence and the locations of petroleum fields suggest that anthropogenic processes related to hydrocarbon production can make subsidence more severe (Morton et al., 2006; Chan and Zoback, 2007; Mallman and Zoback, 2007; Dokka, 2011; Kolker et al., 2011; Yu et al., 2012). Subsidence associated with fluid withdrawal is attributed to reservoir compaction as the effective stress increases with pore pressure reduction associated with production (Geertsma, 1973). Throughout the Louisiana coastal zone, oil and gas fields are pervasive (Figure 1), which were under active production during the 1960–1970s. Morton et al. (2006) and Mallman and Zoback (2007) showed that the locations of higher rates of subsidence coincide with those of oil and gas fields, demonstrating that reservoir compaction associated with active fluid production can certainly increase the rate of subsidence.

An interesting aspect of the subsidence is that after a dramatic reduction of production rate, the subsidence did not stop nor decrease, but accelerated rather significantly for decades (Mallman and Zoback, 2007; Morton and Bernier, 2010). It is known that production-induced compaction processes and

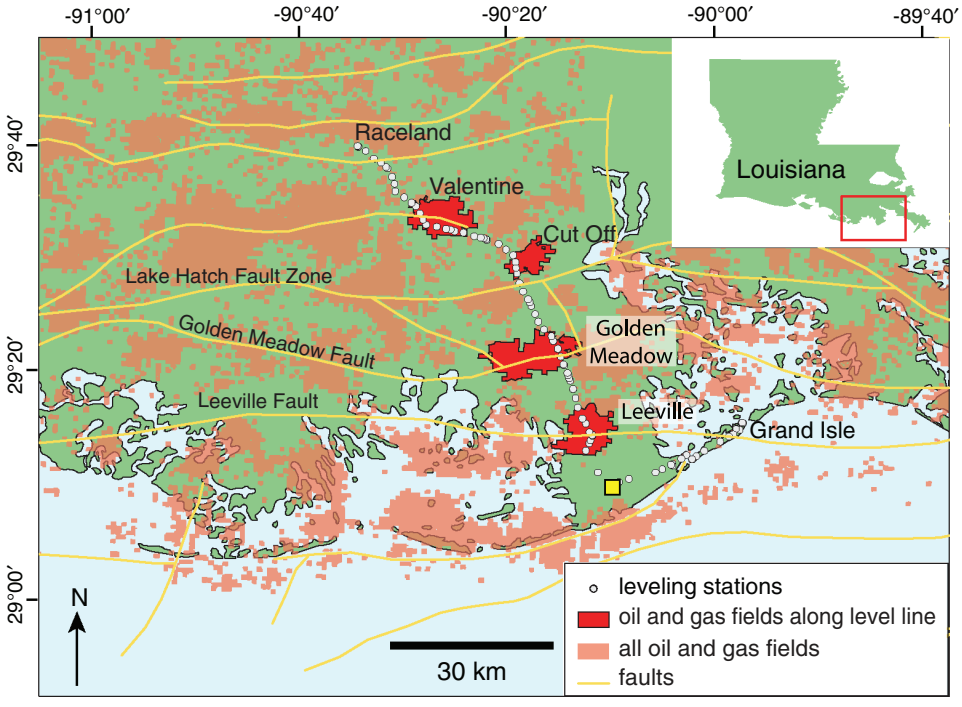

Figure 1. A regional map showing oil and gas fields in the southern coastal zone of Louisiana (modified from Morton et al., 2002). Leveling line used in this study crosses four major fields (Leeville, Golden Meadow, Cut Off, and Valentine). The reference station south of Leeville, used in Figure 2, is marked by a yellow square.

associated subsidence can be time-dependent for various reasons (Schutjens, 1991; Hettema et al., 2002). For example, delayed subsidence is often interpreted as a delayed effective stress change during production, mainly due to slow dissipation of pore pressure within reservoirs (e.g., Baú et al., 1999), or time-dependent creep compaction in reservoir rocks (Hettema et al., 2002). Although the delayed times between production and subsidence vary depending on reservoir conditions, they normally occur over a period of a few years (Hettema et al., 2002).

In the present study, we revisit the subsidence observed in coastal Louisiana, focusing on the apparent accelerated rate of subsidence after reservoir depletion. Because of the long delay between the time of production and subsidence, as well as significant acceleration of subsidence after the end of production, we examine a time-dependent deformation mechanism that might be applicable in the study area of coastal Louisiana, but has not been considered by previous investigators. This mechanism is time-dependent compaction of reservoir-bounding shales driven by the slow drainage of pore fluid from the shale into a severely depleted sand reservoir. In this study, we test this hypothesis using appropriate rheological constitutive laws to investigate whether the compaction in reservoir-bounding shale can be significant enough to induce the observed acceleration of subsidence rate after depletion.

OBSERVATIONS

The subsidence data that we will look at are those measured by benchmark leveling surveys of the National Geodetic Survey. The benchmark stations are located along Louisiana Highway 1 (LA 1) in Lafourche Parish, Louisiana. The leveling line runs from Grand Isle in the south to Raceland in the north, crossing multiple large oil and gas fields (Figure 1). The benchmark surveys were conducted in several epochs, but we focus on leveling data measured in the latest available two epochs: epoch 1 spanning 1965–1982 (17 years) and epoch 2 spanning 1982–1993 (11 years).

Figure 2 shows leveling data and calculated subsidence rates for the two epochs along the line depicted in Figure 1. The line originates at Grand Isle, and this base station is tied to a tide gauge and global positioning system (GPS) station at the Coast Guard Station. The entire line shows a regional subsidence signal on the order of ~5 cm (1.97 inches; e.g., when compared

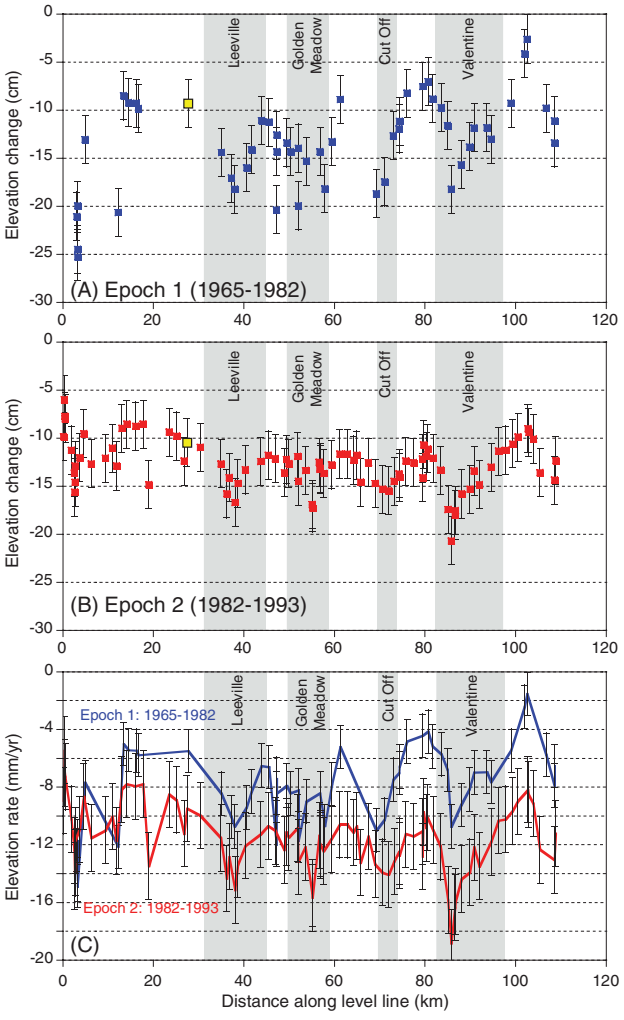

Figure 2. Elevation changes during epoch 1 (1965–1982) (A) and epoch 2 (1982–1993) (B), and the rates of subsidence in the two epochs (C). Over the entire line, subsidence rate is greater in epoch 2 than in epoch 1. The yellow squares in (A) and (B) indicate an arbitrarily selected reference station approximately 8 km (5 mi) south and outside of the projected Leeville field, to estimate the magnitudes of local production-related subsidence signals.

to the elevation of Grand Isle in epoch 2), which might be attributed predominantly to natural processes. In addition, it is evident that there are several localized areas of greater subsidence, which correlate with the four major oil and gas fields (Leeville, Golden Meadow, Cut Off, and Valentine). Morton et al. (2006) carried out an independent analysis on subsidence in this region and obtained virtually the same results. A similar correlation was also observed in the study of Chan and Zoback (2007) in the vicinity of the Lapeyrouse field, west of the present study area.

These localized signals over the oil and gas fields are likely related to production-induced reservoir compaction. In an attempt to isolate the localized subsidence from regional subsidence associated with some of the natural mechanisms discussed above, elevations in Figure 2A, B are compared to an arbitrarily selected reference station indicated by yellow squares, approximately 8 km (4.97 mi) south and outside of the projected Leeville field. During epoch 1, there is approximately 5–10 cm (1.97–3.94 inches) of subsidence over the four fields considered and during epoch 2, there is an additional 5–10 cm (1.97–3.94 inches) of subsidence over these fields.

In Figure 2C, the subsidence rates along the leveling line are shown for the two epochs. The subsidence rates were calculated with respect to the Grand Isle base station, following the approach taken by Shinkle and Dokka (2004), and thus involve the effect of regional subsidence with minimal sea level change. It is evident that the subsidence rate in epoch 2 overall is higher than that in epoch 1. If natural processes during these two epochs did not change during the two epochs, it is inferred that periods of increased subsidence rate should correlate with periods of increased fluid production. However, when production rates from the four fields crossed by the leveling line are compared with the observed subsidence rates, we find the exact opposite. In the oil and gas fields in this region, production peaked during epoch 1 (1965–1982) and decreased markedly afterwards (Figure 3A). During epoch 2, production was only a small fraction of that of epoch 1, because many of the reservoirs were depleted in the second epoch. Some available bottomhole pressure measurements from wells in the Valentine gas field show how drastically pore pressures in reservoirs decreased with time due to active production (Figure 3B). Pore pressures were initially near-hydrostatic (about 33 MPa [4786 psi]) at the inception of epoch 1 and decreased continuously to just a few MPa at the end of production.

The accelerated rate of subsidence in epoch 2 indicates that the fluid withdrawal and associated poroelastic reservoir compaction is not an adequate explanation of the observed subsidence. Morton and Bernier (2010) suggested that the effects of fault reactivation and delayed pore pressure re-equilibration can play a role for the accelerated subsidence during

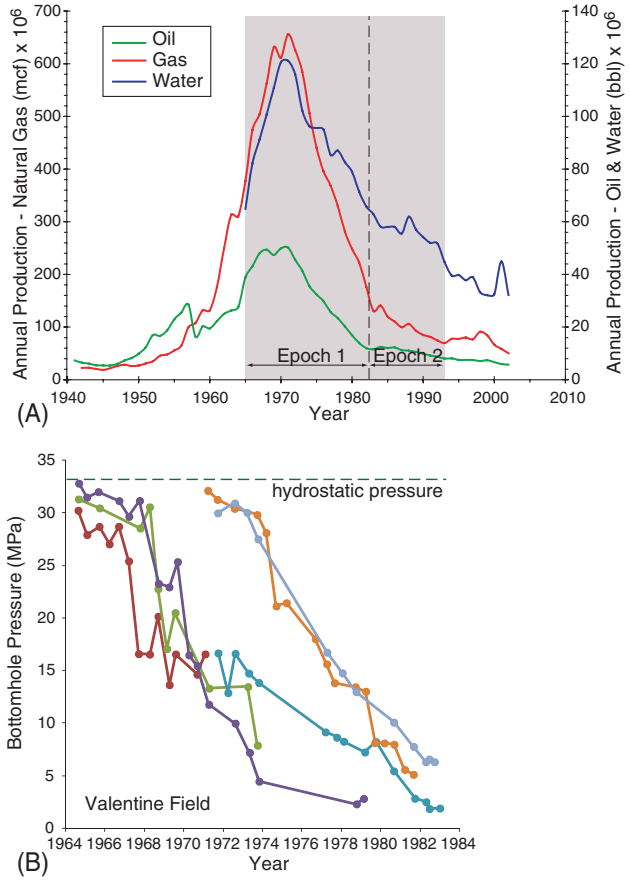

Figure 3. Cumulative annual production data for the Louisiana delta plain (modified from Morton et al., 2005) (A) and an example of bottom-hole pressure in a reservoir of Valentine field (B). Different colors in (B) represent different wells.

epoch 2. Although normal faulting movement can induce subsidence in the vicinity of faults, what we see is accelerated subsidence at a broader scale, not necessarily constrained around faults. Also the entire time span of epoch 1 (17 years) during which most fluids were extracted appears to be sufficiently long for the effect of the pressure depletion to be reflected in the subsidence signals in epoch 1. After the cessation of production, subsidence is expected to stabilize. These speculations led us to look for a more widespread and significant, but much slower, compaction process that has not been previously considered to explain the observed acceleration of subsidence after depletion.

As a possible such process, we propose here time-dependent compaction of reservoir-bounding shales after reservoir has been depleted. Because the shale formation has much lower permeability than the reservoir sands, it does not drain as the reservoir is being depleted, but drains rather slowly over decades, even long after production ceases. To assess the possibility of this process to contribute to the acceleration of postdepletion subsidence, we consider a simple analytic compaction model, in which a few rheological constitutive laws are implemented that can describe compaction in the reservoir system including sands and shales.

COMPACTION MODEL FOR SAND AND SHALE RESERVOIR SYSTEM

Subsidence driven by compaction in the subsurface media can be estimated analytically using solutions developed by Geertsma (1973) and Walsh (2002), which are based on the assumptions that the reservoir is disk-shaped and embedded in an elastic half-space. Key parameters needed to calculate the magnitude of subsidence are the amount of compaction and the dimension of reservoir (size and depth). In this section, we describe a model that can be used to estimate the amounts of compaction in a sand and shale reservoir system because of pore pressure drawdown.

The compaction model consists of a sand reservoir surrounded by bounding-shale formations (Figure 4). In this part of the analysis, we assume that the sand reservoir has a lateral dimension sufficiently large compared to its thickness so that we can assume that compaction occurs in the vertical direction only. This conceptual model applies to sand reservoirs that are inclusions in shale. This model may not be applicable in some cases; for example, a sand reservoir with very weak aquifer support would not be a good candidate. The dimension (or thickness) of the bounding shale is not specified at this point, but we assume that it is sufficiently large so that any pore pressure perturbation after depletion can be limited within the surrounding shale. As fluids are extracted from the reservoir, sands will compact as a response to an increase of the effective stress as pore pressure decreases. A simple but reasonable way of describing the mechanical compaction of sands is by means of poroelasticity. Assuming that deformational properties as well as pore pressure change during production are homogeneous throughout the reservoir, we can

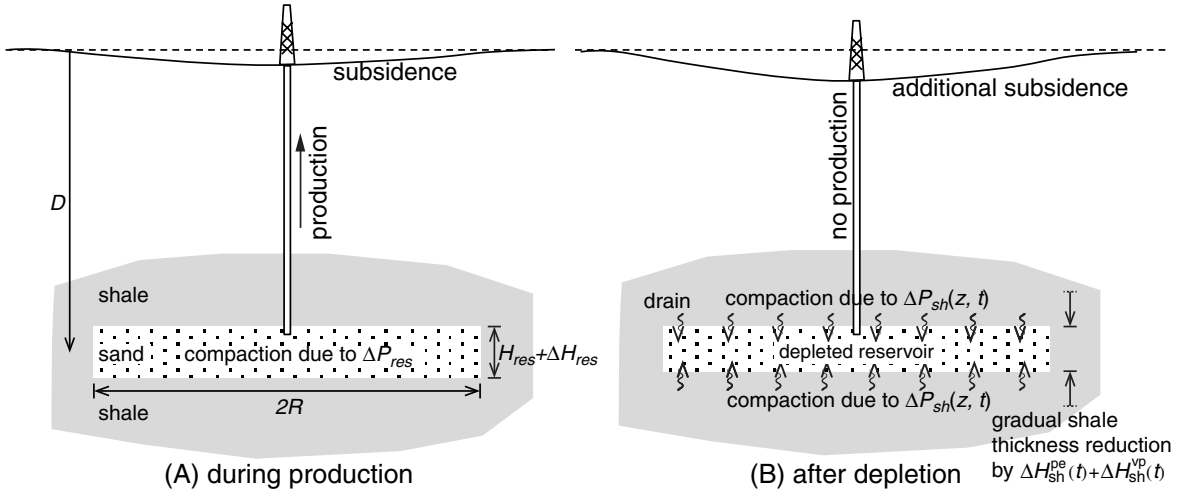

Figure 4. A simple compaction model of sand reservoir (initial thickness H_{res}, width 2R) at a depth of D, embedded within surrounding shale. It is assumed that during epoch 1 (A), pore pressure depletion (ΔP_{res}) in a sand reservoir induces poroelastic compaction, resulting in reduction of the reservoir thickness by ΔH_{res}, and during epoch 2 (B), a slow decrease in pore pressure ($\Delta P_{sh}(z,t)$) in the bounding shale induces shale compaction (in two independent rheological modes: poroelastic [pe] and viscoplastic [vp]), resulting in gradual reduction of shale thickness (indicated by subscript 'sh') by $\Delta H_{sh}^{pe}(t) + \Delta H_{sh}^{vp}(t)$. We assume that compaction occurs in the vertical direction only.

estimate a reduction of reservoir height (ΔH_{res}) associated with decrease in pore pressure (ΔP_{res}) in the form of (Geertsma, 1973)

$$\Delta H_{res} = C_m H_{res} \Delta P_{res} \quad (1)$$

in which C_m is uniaxial compaction coefficient and H_{res} is the initial thickness of the reservoir (Figure 4A).

While pore pressure in the reservoir decreases, however, the extremely low permeability of the confining shale units tends to inhibit pore-fluid flow on the same time scale as the reservoir. Pore fluid from the shale drains to the depleted reservoir slowly over periods of months to years depending on permeability (or diffusivity). This slow process induces time-dependent compaction in the bounding shale as the effective stress in the shale gradually increases with time (Figure 4B).

In order to obtain the amount of compaction in the surrounding shale, we use the one-dimensional hydraulic diffusion equation as a first approximation to derive pore pressure change, assuming that fluid flow occurs only in the vertical direction (Appendix 1). As pore pressure decreases gradually (as given by equation 7 in Appendix 1), the bounding shale compacts with time accordingly.

The mechanism of shale compaction is somewhat more complicated than that of sands, mainly because of complicated poromechanical processes related to the clays contained in shale. In soil mechanics, it is well established that the compaction process in clays is divided into primary and secondary consolidations (Das, 2008). The primary consolidation occurs as a response to an increase in effective stress and a concurrent decrease in excess pore pressure. The secondary consolidation is a time-dependent decrease in volume under constant effective stress, which is also called creep compaction. In fact, a laboratory experimental study attempting to extract the secondary consolidation demonstrated that shale cores recovered from an oil and gas well offshore Louisiana exhibit significant creep compaction resulting from viscous deformation in shale skeletal frame in its room-dry state (Chang and Zoback, 2009). The characteristics of creep compaction, highlighted by irrecoverable strain and strain hardening during creep, indicate that the mode of deformation can be best described by viscoplasticity. Such creep compaction occurs only when the stress condition exceeds the previous maximum (termed preconsolidation stress). Details of the concept and theoretical derivation of viscoplasticity are described in Appendix 2.

Adapting the concepts in soil mechanics to our compaction model, we describe shale compaction with a superposition of these two rheological

constitutive laws: poroelasticity and viscoplasticity. Poroelasticity applies to the shale compaction that occurs as an instantaneous response to an increase of effective stress, whereas viscoplasticity describes creep compaction that occurs as a time-dependent response to a raised constant effective stress over the preconsolidation stress.

The amount of vertical compaction in the upper and lower bounding shales as a poroelastic response to pore pressure diffusion can be calculated by integrating the corresponding vertical strain over the entire vertical distances:

$$\Delta H_{\mathrm{sh}}^{\mathrm{pe}}(t) = 2\int_0^{\infty} C_m \Delta P_{\mathrm{sh}}(z,t)dz = 4\sqrt{\frac{\alpha t}{\pi}} C_m \Delta P_{\mathrm{res}}, \quad (2)$$

in which superscript pe denotes poroelastic, ΔP_{sh} is pore pressure change in shale and thus $C_m \Delta P_{\mathrm{sh}}$ is vertical poroelastic strain; α is hydraulic diffusivity. Poroelasticity predicts compaction of the bounding shale as a function of the square root of time for a given set of material properties and reservoir pressure conditions as pore fluid drains out slowly from the shale.

A constitutive equation is available that can describe the viscoplastic compaction of shale, which was derived from laboratory compaction experiments in the shale cores from offshore Louisiana (Chang and Zoback, 2010). In Appendix 2, we slightly modify the constitutive equation to incorporate it into our shale compaction model. The magnitude of vertical compaction due to the viscoplastic creep strain in the lower and upper bounding shales can be obtained by integrating the strain over depth:

$$\Delta H_{\mathrm{sh}}^{\mathrm{vp}}(t) = 2\int_0^{\infty} \varepsilon_{\mathrm{vp}}(z,t)dz, \quad (3)$$

in which vp denotes viscoplastic, $\varepsilon_{\mathrm{vp}}(z,t)$ is a uniaxial creep strain given by equation 22 in Appendix 2. Thus, the total reduction in vertical height of the reservoir and the surrounding shales can be the sum of the three independent components (equations 1, 2 and 3):

$$\Delta H(t) = \Delta H_{\mathrm{res}} + \Delta H_{\mathrm{sh}}^{\mathrm{pe}}(t) + \Delta H_{\mathrm{sh}}^{\mathrm{vp}}(t). \quad (4)$$

Whereas the first term on the right side for the sand compaction reflects a poroelastic thickness reduction following pore pressure depletion during production in epoch 1, the last two terms for shale compaction reflect a slow thickness reduction associated with an increase in effective stress with time after reservoir depletion in epoch 2.

ESTIMATION OF INDIVIDUAL COMPACTION MECHANISMS

We attempt to apply the compaction model derived previously to one of the reservoirs to estimate the magnitudes of individual compaction mechanisms and examine the possibility of significant time-dependent compaction in the bounding shales after depletion. We choose the Valentine field for this modeling because pore pressure data in the reservoir depth are available and the observed subsidence is most severe along the leveling line. However, many of the parameters needed to evaluate the magnitude of compaction and associated subsidence are still unknown even for this simple one-dimensional compaction model. For these unknown parameters, we utilize data published in the literature.

The lateral extent of the entire Valentine field is about 10 km (6.2 mi) in diameter and roughly equidimensional. However, the geologic structure is complicated with a salt dome at the center of the field (Figure 5), which suggests that the reservoirs are found around the flanks of the salt structure. In fact, the leveling line crosses the southwestern edge of the Valentine field (Figure 1), measuring subsidence due to compaction above that part of the field. We estimate the maximum subsidence associated with production is roughly 8 cm (3.15 inches) during the 17-year period of epoch 1 and 10 cm (0.4 and 3.94 inches) during the 11-year period of epoch 2 (Figure 2), which correspond to the maximum subsidence rates of 5 and 9 mm/yr (0.2 and 0.35 inches/yr), respectively.

It should also be noted that reservoirs appear hydraulically compartmented by sealing faults, in that measured formation pressures were reported to vary depending on the locations of the wells (Mallman and Zoback, 2007). Based on all available information including structural map, fault distribution, and logging data (Pope, 1955), we assume a disk-shaped sand reservoir with 2 km (1.2 miles) in diameter and 100 m (328 ft) in thickness at a depth around 3.3 km

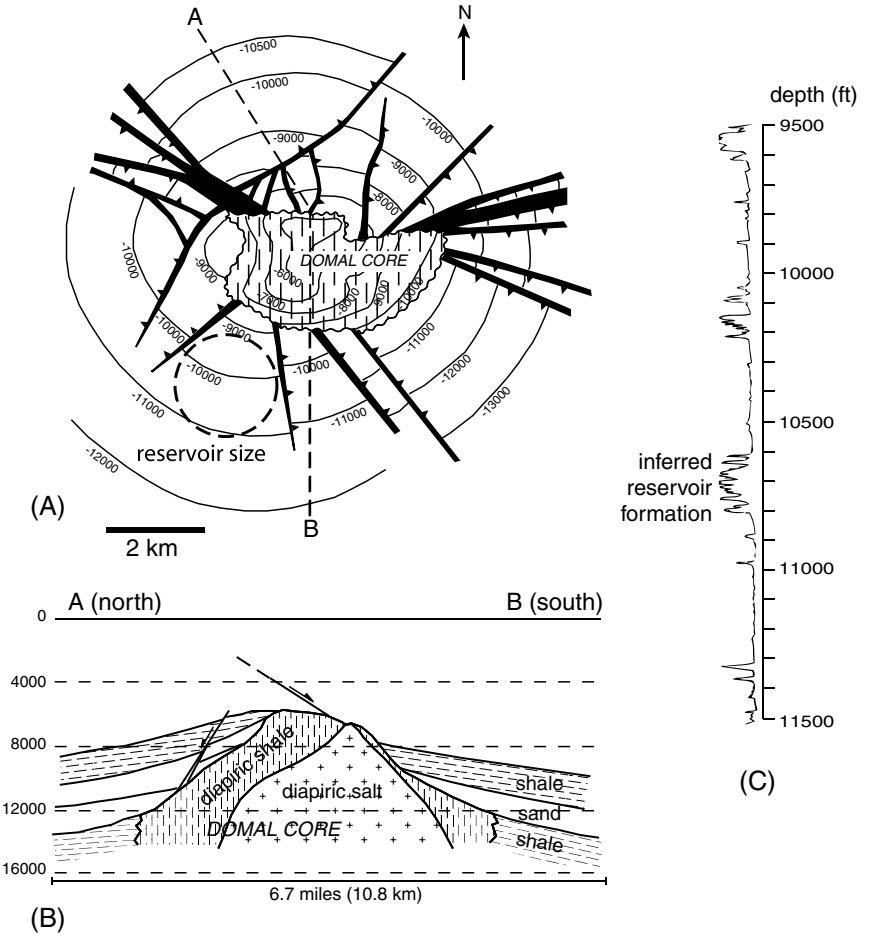

Figure 5. Geologic structure of the Valentine field: map view (A), profile (B) (after Atwater and Forman, 1959), with permission of AAPG and a representative electric log (C) (after Pope, 1955). Valentine field is associated with a salt structure at the center. Depths marked in (A) indicate the top of a sand formation (*Bigenerina humblei*) in feet. Dashed circle in (A) indicates an assumed reservoir for the model study.

(10,827 ft) as shown in Figure 5A, targeting the reservoir where the bottomhole pressure data are available. Thicknesses of over- and underlying shale are not important and not a parameter required for our modeling, as long as pore fluid drainage comes from the surrounding shale. Although the assumed geometry of the reservoir is simple and may differ somewhat from its actual geometry, defining an exact

Table 1. Input Parameters Used in the Compaction Model

Model Parameter	Value	Source
Reservoir depth, D	3300 m (10827 ft)	Atwater and Forman (1959), Morton et al. (2006)
Reservoir diameter, $2R$	2000 m (1.2 miles)	Atwater and Forman (1959)
Reservoir thickness, H_{res}	100 m (328 ft)	Atwater and Forman (1959)
Pore pressure change in reservoir, ΔP_{res}	33 MPa (4786 psi)	Morton et al. (2006)
Uniaxial compaction coefficient, C_m	0.4 GPa^{-1}	This study
Hydraulic diffusivity of shale, α	10^{-6} m^2/sec (10^{-5} ft^2/sec)	Roeloffs (1996), Kwon et al. (2001)
Initial preconsolidation pressure of shale, σ_o	39 MPa (5656 psi)	Assumed to be effective vertical stress
Poisson's ratio, ν	0.3	Assumed
Compression index, C_c	0.082	Chang and Zoback (2010)
Swelling index, C_s	0.0074	Chang and Zoback (2010)
Viscoplastic constant, c_o	10^{-9}	This study (Appendix 2)
Viscoplastic constant, n	40	This study (Appendix 2)

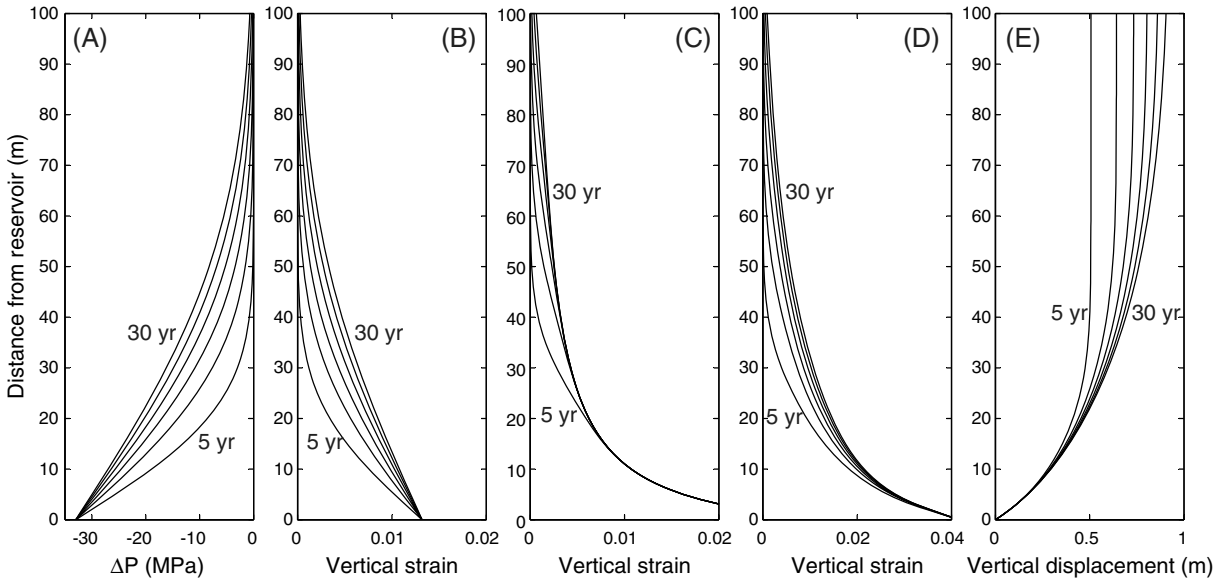

Figure 6. Model results showing (A) pore pressure reduction, (B) poroelastic vertical strain, (C) viscoplastic vertical strain, (D) total vertical strain ($B + C$), and (E) vertical displacement resulting from compaction in the overlying shale for every five years after reservoir depletion as a function of distance from the sand/shale interface. Unitless vertical strain is given as a fraction.

shape of reservoir is less important than defining overall lateral extent of the reservoir, when assessing induced subsidence (Geertsma, 1973).

As shown in Figure 3, pore pressure in this reservoir was near-hydrostatic (33 MPa [4786 psi]) in 1964, and then decreased to just a few MPa with active production during epoch 1. Using the magnitude of subsidence during epoch 1 induced by sand compaction, we back-calculated the uniaxial compaction coefficient (C_m) such that the C_m value used in equation 1 results in the observed surface subsidence during epoch 1. The estimated C_m value is 0.4 GPa^{-1}, which is a reasonable value for semiconsolidated sand reservoirs at the equivalent depth (Geertsma, 1973). All other model parameters are listed in Table 1.

As the sand reservoir is depleted, pore fluid from overlying and underlying shales starts to drain into the depleted sand reservoir. The change in pore pressure and associated vertical strains in the upper bounding shale that would occur after depletion are given in Figure 6 as a function of distance from reservoir for five-year time periods. The same pore pressure change and compaction is expected to occur in the underlying shale. We use a hydraulic diffusivity of 10^{-6} m^2/sec (10^{-5} ft^2/sec), which corresponds to a permeability of 10^{-19} m^2 (10^{-4} mD) with a reasonable range of porosity (5–10%) based on laboratory measurements of Gulf of Mexico shales by Kwon et al. (2001). The change in pore pressure and associated compaction in the shale are severe early in epoch 2, although this partially reflects our assumption that drainage starts only after reservoir depletion. The results show that during the first five years, the lower 30–40 m (100–130 ft) of the overlying shale is markedly compacted. Thereafter, the region of pore pressure change and compaction propagates upward gradually, but is limited to a 100-m (328-ft) interval over a 30-year period. The vertical displacement resulting from the shale compaction is 0.5 m (1.6 ft) for the first five years and increases to approximately 1 m (3.3 ft) during 30 years as shown in Figure 6E.

The magnitudes of individual components of compaction due to different mechanisms in the entire reservoir system (sand reservoir, and the over- and underlying shales) are plotted as a function of time in Figure 7. During epoch 1, the reservoir compacts by 1.3 m (4.3 ft; 1.3% strain) due to pore pressure reduction of 33 MPa (4786 psi). After production ceased, the reservoir thickness remains essentially constant, but subsequent slow drainage of pore fluid from the upper and lower bounding shale causes continuous poroelastic and viscoplastic compaction of

the shale. With the given model parameters, the viscoplastic compaction is larger than the poroelastic compaction. Poroelastic compaction mechanism alone can cause a thickness reduction in shale of ~0.5 m (1.6 ft; comparable to only 40% of sand compaction) in 10 years and ~0.9 m (3.0 ft; 70% of sand compaction) in 30 years. However, the total strain that sums up the poroelastic and viscoplastic compactions yields a thickness reduction comparable to that of the sand reservoir within 10 years.

As shown in Figure 6, thickness reduction in shale occurs in some limited depth range (<100 m [328 ft]) immediately adjacent to the sand reservoir. Thus, the entire compacting formations have a finite height of less than 300 m (984 ft; including sands, and upper and lower bounding shales) at a depth of 3300 m (10,827 ft). According to the Geertsma (1973) approach, the compaction in sands and shales at reservoir depth can be considered as the nucleus of strain, and would propagate through the elastic half-space to induce surface subsidence. Because the amount of compaction increases with time, so does surface subsidence. We use an analytic solution provided by Geertsma (1973) and Walsh (2002) to estimate maximum surface subsidence w_0, which is given by

$$w_0(t) = 2(1-\nu)\Delta H(t)\left(1 - \frac{D}{\sqrt{D^2+R^2}}\right), \qquad (5)$$

in which ν is Poisson's ratio; D and R are depth and half width, respectively, of the reservoir.

Cumulative surface subsidence (calculated using equation 5) resulting from the reservoir sand compaction and that of the bounding shale units are plotted in Figure 8 as a function of time. The slope of the connecting lines is equivalent to an average annual rate of subsidence, which is also plotted as columns in Figure 8. Because we calibrated the value of the uniaxial compaction coefficient (C_m) such that it results in the observed subsidence during epoch 1, it is apparent that the calculation yields the maximum subsidence of 8 cm (3.15 inches) after 17 years of epoch 1, during which only reservoir sand is assumed to compact. This gives a subsidence rate of ~5 mm/yr (0.2 inches/yr), which is identical to our initial estimate. During epoch 2, subsidence continues because of the time-dependent compaction in the upper and lower bounding shales. The shale compaction during the first 10 years after depletion results in a subsidence (additional 8 cm [3.15 inches]) comparable to that due to the sand compaction, as the thickness reduction in the shale becomes

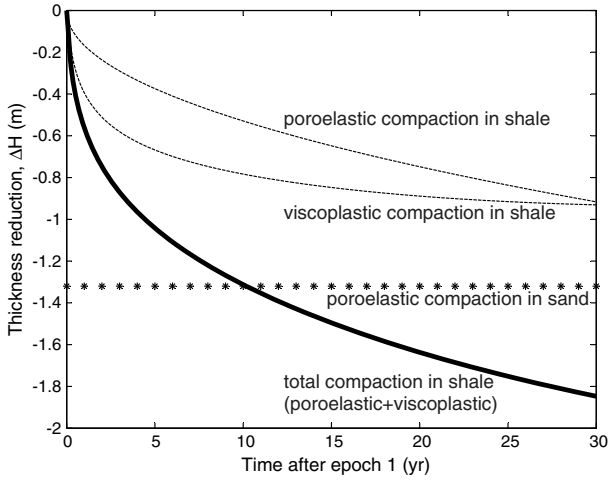

Figure 7. Individual components of compaction in the reservoir system associated with fluid withdrawal from reservoir sand and subsequent pore fluid drainage from the bounding shale. Note that after depletion reservoir thickness remains constant, but slow pore pressure drainage from the bounding shales induces continuous compaction after depletion.

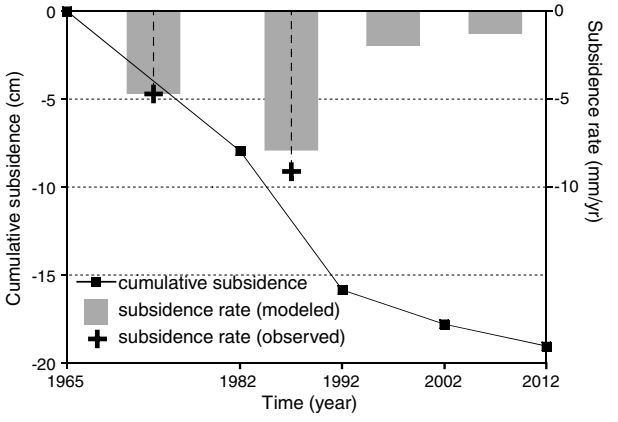

Figure 8. Cumulative subsidence calculated using equation 5. Active production for the 17-year period of epoch 1 induces sand reservoir compaction, which results in the maximum surface subsidence of ~8 cm (3.15 inches). Slow pore pressure drainage from the bounding shale results in an additional ~8 cm (3.15 inches) subsidence for the first 10 years after depletion. Calculated subsidence rate based on the modeled subsidence increases significantly for the first 10 years after depletion, and that decreases markedly afterwards. The calculated subsidence rate is similar to the observed subsidence rate.

comparable to that of reservoir. The subsidence rate during the first 10 years after depletion is 8 mm/yr (0.32 inches/yr), which is somewhat lower than our initial estimate (~9 mm/yr [0.35 inches/yr]) based on the leveling data shown in Figure 2, but clearly higher than that during epoch 1. This result demonstrates that the time-dependent compaction of reservoir-bounding shale after active production is a plausible mechanism that may accelerate subsidence even after depletion. Based on our shale compaction model, the postdepletion subsidence will markedly slow down afterwards. For the subsequent decades, the subsidence rates become lower than 2 mm/yr (0.08 inches/yr), implying gradual stabilization as pore pressure drainage is reduced. Indeed, recent studies that analyzed post-1990s subsidence showed stabilization of subsidence in the region (Morton and Bernier, 2010; Kolker et al., 2011), which agrees with our model results.

DISCUSSION AND CONCLUSIONS

We utilized a relatively simple model (using a simple reservoir geometry with constant material properties) to demonstrate the significant shale compaction that may be responsible for the observed acceleration in subsidence rate after depletion. The benefit of using such a simple model is that we can implement a variety of known constitutive laws in analytic ways, so we can understand the respective contributions of individual compaction mechanisms. It is obvious, however, that the modeling results may have some ranges of uncertainty arising from somewhat simplistic assumptions imposed in our model. For example, we decomposed compacting media (reservoir and reservoir-bounding shale) chronologically before and after depletion. In reality, it is likely that the bounding shale starts draining as soon as the equilibrium in pore pressure breaks down while fluids are being produced from the reservoir. Thus, it is likely that the surrounding shales start to compact during production and contribute to the subsidence during epoch 1. Unfortunately, we do not have an analytic way to deal with such a coupled process, and we think that it can be done with help of numerical analysis. Because the major driving force for pore fluid drainage is the pressure contrast between the sand reservoir and the surrounding shales, however, pore pressure diffusion from the bounding shale would be of second order importance during the early stage of production when pore pressure drawdown in the reservoir is not severe.

We incorporated the viscoplastic compaction component in shale based on laboratory observations on how dry frame of shale compacts with time at constant effective stresses (Chang and Zoback, 2009, 2010). The magnitudes of viscoplastic component may vary depending on the types of shale, and our modeling results are subject to change accordingly. However, we interpret that the viscoplastic deformation in shale is largely correlated to the role of clay content, which exhibits time-dependent creep. The viscoplastic constitutive equation used in our calculation was developed based on laboratory tests in poorly consolidated shale offshore Louisiana with approximately 50% or larger clay content (Losh et al., 1999), which is typical reservoir-bounding shale expected to be found in coastal Louisiana as well.

Some reservoir sands are reported to exhibit creep behavior in the same manner as observed in shale, but with much lower magnitudes than shale (Hagin and Zoback, 2004). Then the reservoir itself may exhibit time-lagged compaction, which can contribute somewhat to the subsidence after depletion. However, this is expected to occur quite quickly and can be difficult to distinguish from the compaction of the reservoir with production (Hagin and Zoback, 2007).

Overall, we showed that slow drainage of pore fluid from the surrounding shale to a depleted reservoir can induce a significant time-dependent compaction and associated subsidence. It is worth emphasizing that the subsidence rate due only to reservoir sand compaction depends largely on the production rate. A faster production rate would result in a higher rate of subsidence. However, the subsidence rate caused by the compaction of the surrounding shale depends mainly on properties of shale, that is, the permeability and viscoplastic properties. We demonstrated that the postdepletion subsidence can be significant with severe depletion.

As the pore fluid in the shale drains into the depleted reservoir, the shale compaction propagates upwards from the sand/shale interface as the shale pore pressure diffuses with time. The maximum compaction zone in the bounding shale moves upwards at a rate principally depending on the permeability of

the shale and time. Because compaction in reservoir-bounding formations often cause well-casing damage (Fredrich et al., 2000), information on the casing damage could potentially be used to better constrain permeability estimates in shale.

APPENDIX 1: PORE PRESSURE DRAIN IN THE BOUNDING SHALE

The governing equation of the one-dimensional diffusion for pore pressure change in shale (ΔP_{sh}) is

$$\frac{\partial^2(\Delta P_{sh})}{\partial z^2} = \frac{1}{\alpha}\frac{\partial(\Delta P_{sh})}{\partial t}, \tag{6}$$

in which α is hydraulic diffusivity of shale, z is vertical coordinate, and t is time. A general solution for equation 6 is known (Talwani and Acree, 1985) and requires a boundary condition to be completed. Because what drives the pore pressure diffusion is a large pressure contrast at the boundary between the reservoir sands and the bounding shale, we assume that pore fluid in the shale starts to drain when the pore pressure contrast is at maximum (i.e., when the reservoir pore pressure minimizes). Although, in reality, shale pore pressure may drain as soon as the equilibrium state is lost, the effect of pressure diffusion is maximized when the pressure contrast is greatest. With that boundary condition, the pore pressure change in the bounding shale is obtained in the form of

$$\Delta P_{sh}(z,t) = \Delta P_{res} erfc\left(\frac{z}{2\sqrt{\alpha t}}\right), \tag{7}$$

in which $erfc$ is the complementary error function, z is the distance from the boundary between the reservoir and the shale, and ΔP_{res} is the maximum pressure drawdown in the sand reservoir. Equation 7 represents a pore pressure change (or equivalently, effective stress change) in the bounding shale as a function of space and time as pore fluid drains.

APPENDIX 2: VISCOPLASTIC COMPACTION OF SHALE

Derivation of Constitutive Equation

We describe here a viscoplastic constitutive model for hydrostatically loaded shale, and then convert it into that for the uniaxial strain regime used in this study. The viscoplastic constitutive model is valid for describing the time-dependent deformation of the dry skeletal frame of shale that is an inherent property of the material (Chang and Zoback, 2009). Much of the derivation procedure follows that presented in Chang and Zoback (2010).

The derivation starts from Perzyna's rule of viscoplastic flow (Perzyna, 1963):

$$\dot{\varepsilon}_{ij}^{vp} = \langle \varphi(F) \rangle \frac{\partial f_d}{\partial \sigma_{ij}}, \tag{8}$$

in which $\dot{\varepsilon}^{vp}$ is viscoplastic strain rate; F is overstress function; φ is viscoplastic flow function; f_d is dynamic yield function; and $\langle\rangle$ is a Macaulay bracket, with which $\langle\varphi(F)\rangle = 0$ for $F \le 0$ and $\langle\varphi(F)\rangle = \varphi(F)$ for $F > 0$. The overstress function F is a normalized distance between the current stress and the stress on the static yield surface, simply meaning a measure of how much the current stress is beyond the yield stress (or preconsolidation stress). Here, we define the viscoplastic flow function together with overstress function as

$$\varphi(F) = c_o\left(\left(\frac{f_d}{f_s}\right)^n - 1\right), \tag{9}$$

in which c_o and n are viscoplastic material constants and f_s is the static yield function. With such a definition, if dynamic and static yield functions are identical (i.e., no viscous rheology), the viscoplastic strain rate becomes zero; and if the dynamic yield function exceeds the static yield, the viscoplastic strain rate has some value determined by the material constants c_o and n, which are determined from experimental data.

To define static and dynamic yield functions, we use the modified Cambridge Clay model (Roscoe and Burland, 1968) of the form

$$M^2p^2 - M^2\sigma_o p + q^2 = 0, \tag{10}$$

in which p is the mean normal stress ($\equiv (\sigma_1 + \sigma_2 + \sigma_3)/3$), and q is the deviatoric stress ($\equiv ((\sigma_1 - \sigma_2)^2 + (\sigma_2 - \sigma_3)^2 + (\sigma_3 - \sigma_1)^2)^{1/2}/\sqrt{2}$); M is the slope of the critical state line in $p - q$ space; and σ_o is the intersection between the static yield surface and p-axis (preconsolidation pressure). The yield surface of the modified Cambridge Clay model is an elliptical shape in $p - q$ space, the size for which is determined by σ_o. The preconsolidation pressure is nothing but the yield point in the hydrostatic loading condition that defines the threshold boundary between elastic and plastic regimes (i.e., $f_s = \sigma_o$ for the hydrostatic loading condition). However, if the material behavior is viscous, the threshold boundary varies depending on strain rate, although the actual preconsolidation stress is fixed. Thus, we define the dynamic yield point as the current stress that can be retained by an instantaneous loading with some strain rate, i.e., $f_s = \sigma$.

Substituting the flow function (equation 9) and the stress conditions defining dynamic and static yield points into Perzyna's viscoplastic flow rule, we get

$$\dot{\varepsilon}^{vp} = c_o\left(\left(\frac{\sigma}{\sigma_o}\right)^n - 1\right). \tag{11}$$

The implication of equation 11 can be interpreted as follows. If the stress (σ) is raised above the preconsolidation stress (σ_o), time-dependent strain (creep) occurs. During creep, rock actually compacts with time as it undergoes creep strain, which consequently raises the preconsolidation stress. When the preconsolidation stress reaches the current stress level (σ), creep ends. Thus, the preconsolidation pressure is also a function of viscoplastic strain, because it evolves with the viscoplastic strain that the rock experiences.

To apply the viscoplastic constitutive equation (equation 11) to the subsidence problem in which we are interested, it is convenient to have a viscoplastic strain (ε^{vp}) as a function of time and the stress condition. This requires another independent equation to eliminate one of the two variables (either $\dot{\varepsilon}^{vp}$ or σ_o). For

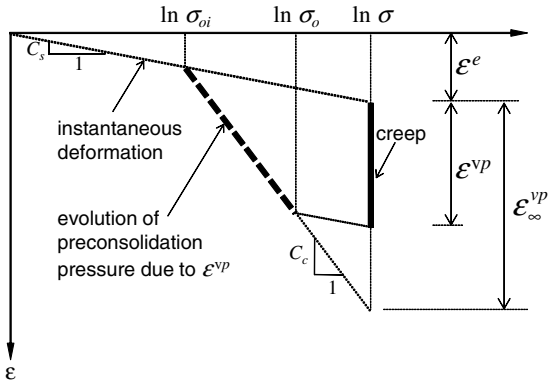

Figure 9. Schematic of stress-strain relations, showing creep strain at a constant stress (σ) when stress is raised instantaneously above the initial preconsolidation stress (σ_{oi}) and the locus of preconsolidation stress evolution (σ_o) as rock creeps. ε^e is elastic strain, ε^{vp} is viscoplastic strain as a function of time, and ε^{vp}_∞ is total viscoplastic strain expected at a stress σ.

this, we use an idealized stress–strain curve in $\varepsilon - \ln \sigma$ space as is typically used in conventional soil mechanics (Figure 9). When an elastic–plastic material (with its initial preconsolidation pressure σ_{oi}) is compressed, it first deforms elastically (with the slope of the line being C_s called the swelling index) until the pressure reaches the initial preconsolidation pressure, and thereafter it follows the inviscid compaction line (with the slope being C_c called the compression index) as pressure increases further. As the rock experiences a plastic strain, the preconsolidation pressure evolves progressively, following the inviscid compaction stress–strain line.

The strain-hardening concept can be extended to the case of elasto-viscoplastic deformation. That is, the viscoplastic strain causes the increase in preconsolidation pressure for elasto-viscoplastic material. As the viscoplastic strain is time dependent, so is the evolution of preconsolidation pressure. In Figure 9, the creep strain ε^{vp} that occurs at stress σ for a given period of time corresponds to the increase in preconsolidation pressure from σ_{oi} to σ_o. If creep continues with time, the preconsolidation pressure keeps increasing until it reaches eventually to σ. A relation between viscoplastic strain and preconsolidation stress can be readily derived in the form of

$$\varepsilon^{vp}_\infty - \varepsilon^{vp} = (C_c - C_s)\ln\frac{\sigma}{\sigma_o}, \tag{12}$$

in which ε^{vp}_∞ is the total viscoplastic strain at the end of consolidation at stress level σ. The implication of equation 12 is that a total amount of viscoplastic strain ($\varepsilon^{vp}_\infty - \varepsilon^{vp}$) is expected when a material of preconsolidation stress σ_o is loaded hydrostatically to a stress $\sigma(> \sigma_o)$. Thus, if the pressure is increased instantaneously to stress σ, the creep strain as a function of time will follow the instantaneous loading. At the same time, the preconsolidation stress will evolve with the creep strain ε^{vp}. In other words, it is possible to say that the creep strain is a result of time-dependent evolution of the preconsolidation stress, and vice versa.

A differential equation can be derived by combining equations 11 and 12 and eliminating the σ/σ_o term:

$$\dot{\varepsilon}^{vp} = c_o(e^{A\varepsilon^{vp}_\infty}e^{-A\varepsilon^{vp}} - 1), \tag{13}$$

in which $A = n/(C_c - C_s)$. Solving the differential equation gives a time function of ε^{vp} in the form of

$$\varepsilon^{vp}(t) = \frac{1}{A}\ln(e^{A\varepsilon^{vp}_\infty} + e^{-AC_1}e^{-Ac_o t}), \tag{14}$$

in which C_1 is a constant that can be determined by an initial condition. Let us assume that, at $t = 0$, the preconsolidation pressure reaches σ_o and a total cumulative amount of viscoplastic strain that contributes to increase the preconsolidation pressure from σ_{oi} to σ_o is ε^{vp}_o, that is,

$$\varepsilon^{vp}(t=0) = \frac{1}{A}\ln(e^{A\varepsilon^{vp}_\infty} + e^{-AC_1}) = \varepsilon^{vp}_o, \tag{15}$$

from which we can determine the constant C_1. Then we get

$$\varepsilon^{vp}(t) = \frac{1}{A}\ln(e^{A\varepsilon^{vp}_\infty} + (e^{A\varepsilon^{vp}_o} - e^{A\varepsilon^{vp}_\infty})e^{-Ac_o t}). \tag{16}$$

Note that, at $t = 0$, equation 16 gives $\varepsilon^{vp}(0) = \varepsilon^{vp}_o$, which is viscoplastic strain accumulated before $t = 0$. If we subtract the initial strain ε^{vp}_o from equation 16, we can obtain creep strain ε_{vp} as a function of time that contributes the increase of preconsolidation stress from σ_o to σ, which is in the form of

$$\begin{aligned}\varepsilon_{vp}(t) &= \varepsilon^{vp}(t) - \varepsilon^{vp}_o \\ &= \frac{1}{A}\ln(e^{A\varepsilon^{vp}_\infty} + (e^{A\varepsilon^{vp}_o} - e^{A\varepsilon^{vp}_\infty})e^{-Ac_o t}) - \frac{1}{A}\ln(e^{A\varepsilon^{vp}_o}) \\ &= \frac{1}{A}\ln(e^{A(\varepsilon^{vp}_\infty - \varepsilon^{vp}_o)} + (1 - e^{A(\varepsilon^{vp}_\infty - \varepsilon^{vp}_o)})e^{-Ac_o t}).\end{aligned} \tag{17}$$

Using equation 12, equation 17 can be expressed as

$$\begin{aligned}\varepsilon_{vp}(t) &= \frac{1}{A}\ln\left(\left(\frac{\sigma}{\sigma_o}\right)^n + \left(1 - \left(\frac{\sigma}{\sigma_o}\right)^n\right)e^{-Ac_o t}\right) \\ &= \frac{1}{A}\ln\left(e^{-Ac_o t} + (1 - e^{-Ac_o t})\left(\frac{\sigma}{\sigma_o}\right)^n\right).\end{aligned} \tag{18}$$

Note that, in equation 18, viscoplastic strain vanishes when σ is equal to σ_o. In addition, as time approaches to infinity, the amount of viscoplastic strain converges to a finite value,

$$\varepsilon_{vp}|_{t\to\infty} = \frac{1}{A}\ln\left(\frac{\sigma}{\sigma_o}\right)^n, \tag{19}$$

which depends on stress condition raised over the preconsolidation stress.

Because equation 18 represents volumetric creep strain derived for the hydrostatic loading condition, an appropriate conversion is necessary to use it for the uniaxial compaction condition, which yields (Teeuw, 1971)

$$\varepsilon_{vp}(t) = \frac{1}{3}\left(\frac{1+\nu}{1-\nu}\right)\frac{1}{A}\ln\left(e^{-Ac_o t} + (1 - e^{-Ac_o t})\left(\frac{\sigma}{\sigma_o}\right)^n\right), \tag{20}$$

in which ν is Poisson's ratio. That is, when pore pressure at a depth z in the bounding shale decreases instantly by $\Delta P_{sh}(z)$,

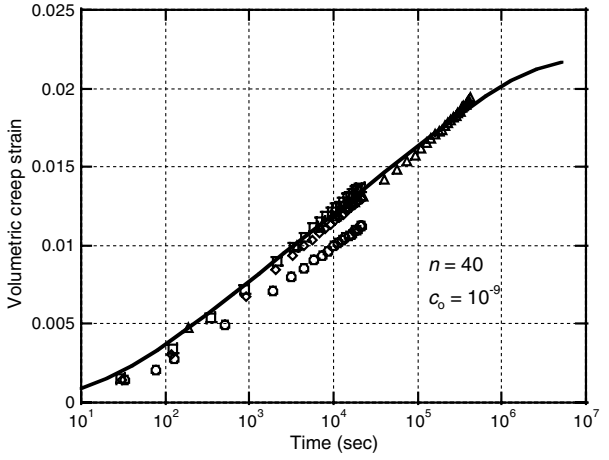

Figure 10. Volumetric creep strains as a function of time at a constant hydrostatic stress level (30 MPa [4351 psi]) after 5 MPa (725 psi) instantaneous stress increase. Different symbols indicate experimental data obtained from different shale samples. A best fitting curve (solid line) using equation 18 yields values of viscoplastic material constants, n and c_o, which will be used in our model study.

the resultant amount of creep strain (ε_{vp}) is given as a function of time:

$$\varepsilon_{vp}(z,t) = \frac{1}{3}\left(\frac{1+\nu}{1-\nu}\right) \times \frac{1}{A}\ln\left[e^{-Ac_o t} + (1-e^{-Ac_o t})\left(1-\frac{\Delta P_{sh}(z)}{\sigma_o}\right)^n\right]. \quad (21)$$

To implement this viscoplastic model in the reservoir shale condition where pore pressure changes gradually, a couple of practical points have to be taken into account. First, because the pore pressure changes gradually with time due to diffusion, the total accumulated creep strain for a certain period is the sum of small creep strains that follow small instantaneous elements of pore pressure change up to that time. Second, as the shale compacts because of viscoplastic strain, the preconsolidation stress evolves gradually following the inviscid compaction trend. All these processes can be implemented using a numerical summation of small creep strains, which is expressed as

$$\varepsilon_{vp}(z,t) = \frac{1}{3}\left(\frac{1+\nu}{1-\nu}\right)\frac{1}{A}\sum_i \ln\left[e^{-Ac_o(t-\tau_i)} + (1-e^{-Ac_o(t-\tau_i)}) \times \left(1-\frac{\Delta P_{sh}(z,\tau_i) - \Delta P_{sh}(z,\tau_{i-1})}{\sigma_{o,i}}\right)^n\right], \quad (22)$$

in which $\sigma_{o,i} = \sigma_{o,i-1}\exp(\varepsilon_{vp,i-1}/C_c)$, representing the evolution of preconsolidation stress.

Determination of Model Parameters

We use our laboratory data from creep experiments in the Gulf of Mexico shale (Chang and Zoback, 2009) to determine the model parameters. The shale was recovered from a depth of 2.26 km (7414.7 ft), offshore Louisiana. It is typical unconsolidated shale with a porosity of 27% and approximate clay content higher than 50%. Details of other shale properties are described in Chang and Zoback (2009).

The volumetric creep strains as a function of time were obtained from several experiments, in which we first applied rapid pressurization at a rate of 5 MPa/min (725 psi/min) and kept the pressure constant for about six hours up to five days. From regression analysis on the slope of the creep curves using equation 18, the values of n and c_o were determined to be 40 and 10^{-9}, respectively (Figure 10).

REFERENCES CITED

Atwater, G. I., and M. J. Forman, 1959, Nature of growth of southern Louisiana salt domes and its effect on petroleum accumulation: AAPG Bulletin, v. 43, p. 2592–2622.

Baú, D., G. Gambolati, and P. Teatini, 1999, Residual land subsidence over depleted gas fields in the Northern Adriatic Basin: Environmental & Engineering Geoscience, v. 5, p. 389–405.

Chan, A. W., and M. D. Zoback, 2007, The role of hydrocarbon production on land subsidence and fault reactivation in the Louisiana coastal zone: Journal of Coastal Research, v. 233, no. 3, p. 771–786, doi: 10.2112/05-0553.

Chang, C., and M. D. Zoback, 2009, Viscous creep in room-dried unconsolidated Gulf of Mexico shale (I): Experimental results: Journal of Petroleum Science and Engineering, v. 69, nos. 3–4, p. 239–246, doi: 10.1016/j.petrol.2009.08.018.

Chang, C., and M. D. Zoback, 2010, Viscous creep in room-dried unconsolidated Gulf of Mexico shale (II): Development of a viscoplasticity model: Journal of Petroleum Science and Engineering, v. 72, nos. 1–2, p. 50–55, doi: 10.1016/j.petrol.2010.03.002.

Das, B. M., 2008, Advanced soil mechanics: New York, Taylor & Francis, 567 p.

Dokka, R. K., 2006, Modern-day tectonic subsidence in coastal Louisiana: Geology, v. 34, no. 4, p. 281–284, doi: 10.1130/G22264.1.

Dokka, R. K., 2011, The role of deep processes in late 20th century subsidence of New Orleans and coastal areas of southern Louisiana and Mississippi: Journal of Geophysical Research, v. 116, p. B06403, doi: 10.1029/2010JB008008.

Fearnley, S. M., M. D. Miner, M. Kulp, C. Bohling, and S. Penland, 2009, Hurricane impact and recovery shoreline change analysis of the Chandeleur Islands, Louisiana, USA: 1855 to 2005: Geo-Marine Letters, v. 29, no. 6, p. 455–466, doi: 10.1007/s00367-009-0155-5.

Fredrich, J. T., J. G. Arguello, G. L. Deitrick, and E. D. Rouffignac, 2000, Geomechanical modeling of reservoir compaction, surface subsidence, and casing damage at the Belridge diatomite field: SPE Reservoir Evaluation & Engineering, v. 3, p. 348–359.

Geertsma, J., 1973, Land subsidence above compacting oil and gas reservoirs: Journal of Petroleum Technology, v. 25, no. 6, p. 734–744, doi: 10.2118/3730-PA.

Hagin, P. N., and M. D. Zoback, 2004, Viscous deformation of unconsolidated reservoir sands (Part I): Time-dependent deformation, frequency dispersion and attenuation: Geophysics, v. 69, no. 3, p. 731–741, doi: 10.1190/1.1759459.

Hagin, P. N., and M. D. Zoback, 2007, Predicting and monitoring long-term compaction in unconsolidated reservoir sands using a dual power law model: Geophysics, v. 72, no. 5, p. E165–E173, doi: 10.1190/1.2751501.

Hettema, M., E. Papamichos, and P. Schutjens, 2002, Subsidence delay: Field observations and analysis: Oil & Gas Science and Technology - Revue d'IFP Energies nouvelles, v. 57, no. 5, p. 443–458, doi: 10.2516/ogst:2002029.

Kolker, A. S., M. A. Allison, and S. Hameed, 2011, An evaluation of subsidence rates and sea level variability in the northern Gulf of Mexico: Geophysical Research Letters, v. 38, p. L21404, doi: 10.1029/2011GL049458.

Kwon, O., A. K. Kronenberg, A. F. Gangi, and B. Johnson, 2001, Permeability of Wilcox shale and its effective pressure law: Journal of Geophysical Research, v. 106, no. B9, p. 19339–19353, doi: 10.1029/2001JB000273.

Losh, S., L. Eglinton, M. Schoell, and J. Wood, 1999, Vertical and lateral fluid flow related to a large growth fault, South Eugene Island Block 330 field, offshore Louisiana: AAPG Bulletin, v. 83, p. 244–276.

Mallman, E. P., and M. D. Zoback, 2007, Subsidence in the Louisiana Coastal Zone due to hydrocarbon production: Journal of Coastal Research, v. SI 50, p. 443–449.

Meckel, T. A., U. S. T. Brink, and S. J. Williams, 2006, Current subsidence rates due to compaction of Holocene sediments in southern Louisiana: Geophysical Research Letters, v. 33, p. L11403, doi: 10.1029/2006GL026300.

Morton, R. A., N. A. Buster, and M. D. Krohn, 2002, Subsurface controls on historical subsidence rates and associated wetland loss in southcentral Louisiana: Transactions Gulf Coast Association of Geological Societies, v. 52, p. 767–778.

Morton, R. A., G. Tiling, and N. F. Ferina, 2003, Causes of hotspot wetland loss in the Mississippi delta plain: Environmental Geosciences, v. 10, no. 2, p. 71–80, doi: 10.1306/eg100202007.

Morton, R. A., J. C. Bernier, J. A. Barras, and N. F. Ferina, 2005, Rapid subsidence and historical wetland loss in the Mississippi Delta Plain: Likely causes and future implications: USGS Open File 2005-1216, 116 p.

Morton, R. A., J. C. Bernier, and J. A. Barras, 2006, Evidence of regional subsidence and associated interior wetland loss induced by hydrocarbon production, Gulf Coast region, USA: Environmental Geology, v. 50, no. 2, p. 261–274, doi: 10.1007/s00254-006-0207-3.

Morton, R. A., and J. C. Bernier, 2010, Recent subsidence-rate reductions in the Mississippi Delta and their geological implications: Journal of Coastal Research, v. 26, no. 3, p. 555–561, doi: 10.2112/JCOASTRES-D-09-00014R1.1.

Penland, S., L. Wayne, L. D. Britsch, S. J. Williams, A. D. Beall, and V. C. Butterworth, 2000, Process classification of coastal land loss between 1932 and 1990 in the Mississippi River Delta Plain, southeastern Louisiana: USGS Open File 00–418, 1 sheet.

Perzyna, P., 1963, The constitutive equations for rate sensitive plastic materials: Quarterly of Applied Mathematics, v. 20, p. 321–332.

Pope, D. E., 1955, Comparison of the Harang and Hackberry facies in south Louisiana: Transactions of the Gulf Coast Association of Geological Societies, v. 5, p. 153–163.

Roeloffs, E., 1996, Poroelastic techniques in the study of earthquake-related hydrologic phenomena: Advances in Geophysics, v. 37, p. 135–195, doi: 10.1016/S0065-2687(08)60270-8.

Roscoe, K. H., and J. B. Burland, 1968, On the generalized stress-strain behaviour of wet clay: *in* J. Heyman, and F. P. Leckie, eds.: Engineering Plasticity, p. 535–609.

Scardina, A. D., J. A. Nunn, R. H. Pilger, Jr., and Anonymous, 1981, Subsidence and flexure of the lithosphere in the north Louisiana salt basin: AGU Eos Transactions, p. 391.

Schutjens, P. M. T. M., 1991, Experimental compaction of quartz sand at low effective stress and temperature conditions: Journal of the Geological Society, London, v. 148, no. 3, p. 527–539, doi: 10.1144/gsjgs.148.3.0527.

Shinkle, K. D., and R. K. Dokka, 2004, Rates of vertical displacement at benchmarks in the lower Mississippi Valley and the northern Gulf Coast: NOAA Technical Report, 50, p. 135.

Talwani, P., and S. Acree, 1985, Pore pressure diffusion and the mechanism of reservoir-induced seismicity: Pure and Applied Geophysics, v. 122, no. 6, p. 947–965, doi: 10.1007/BF00876395.

Teeuw, D., 1971, Prediction of formation compaction from laboratory compressibility data: SPE Journal, v. 11, p. 263–268.

Törnqvist, T. E., D. J. Wallace, J. E. A. Storms, J. Wallinga, R. L. van Dam, M. Blaauw, M. S. Derksen, C. J. W. Klerks, C. Meijneken, and E. M. A. Snijders, 2008, Mississippi Delta subsidence primarily caused by compaction of Holocene strata: Nature Geoscience, v. 1, p. 173–176, doi: 10.1038/ngeo129.

Walsh, J. B., 2002, Subsidence above a planar reservoir: Journal of Geophysical Research, v. 107, p. ETG 6-1–ETG 6-9.

Yu, S.-Y., T. E. Törnqvist, and P. Hu, 2012, Quantifying Holocene lithospheric subsidence rates underneath the Mississippi Delta:Earth and Planetary Science Letters, v. 331–332, p. 21–30, doi: 10.1016/j.epsl.2012.02.021.